Earth, Planets and Space

EXPRESS LETTER

Open Access

Deep low-frequency earthquake activity associated with the 2018 eruptions in the Kirishima volcanic complex, Japan

Ryo Kurihara[1,2*] and Aitaro Kato[1]

Abstract

Deep low-frequency (DLF) earthquakes have occurred at depths of 10–30 km in the Kirishima volcanic complex, Japan. Here, we investigate the DLF earthquake activity that was associated with the 2018 eruptions, compare these DLF earthquakes with those associated with the 2011 eruptions, and provide inferences on magmatic fluid ascension during these two eruptions. We apply a new matched-filter method to the continuous waveform data from the 2017–2018 period to comprehensively detect the DLF earthquake activity surrounding the 2018 eruptions. This new method can detect microearthquakes using a single seismic station based on an index that is computed as the product of mutual information and the correlation coefficient to measure the similarity between the template and target waveforms. We perform the same analysis using the 2010–2011 waveform data for comparison with the DLF earthquake activity associated with the 2011 eruptions. We detect 75 DLF earthquakes at approximately 25 km depth during the 2017–2018 period, whereas we detect 1302 DLF earthquakes at similar depths during the 2010–2011 period. Although the number of detected 2017–2018 events is small, we identify two swarms of DLF earthquake activity in March and July 2017. The March 2017 swarm coincides with the appearance of mud pots and jet fumaroles at the surface, and the July 2017 swarm coincides with the initiation of crustal deformation, which indicates the inflation of a deep magma reservoir. Furthermore, the occurrence rate of DLF earthquakes increased slightly after the March 2018 eruptions. Although the occurrence rate of DLF earthquakes associated with the 2018 eruptions was much lower than that associated with the 2011 eruptions, the slight increase in DLF earthquakes during the 2018 eruptions implies a connection between the deep magmatic fluid ascension and shallow volcanic unrest in 2018, which is similar to that observed during the 2011 eruptions. Such a close temporal relationship between the DLF earthquakes and surface volcanic activity suggests that the pressure disturbance within volcanic conduits propagates rapidly from depth.

Keywords: Matched-filter technique, Low-frequency earthquakes, Mutual information, Kirishima Volcanic complex

*Correspondence: kurihara@onken.odawara.kanagawa.jp

[1] Earthquake Research Institute, The University of Tokyo, 1-1-1 Yayoi, Bunkyo, Tokyo 113-0032, Japan
Full list of author information is available at the end of the article

Graphical Abstract

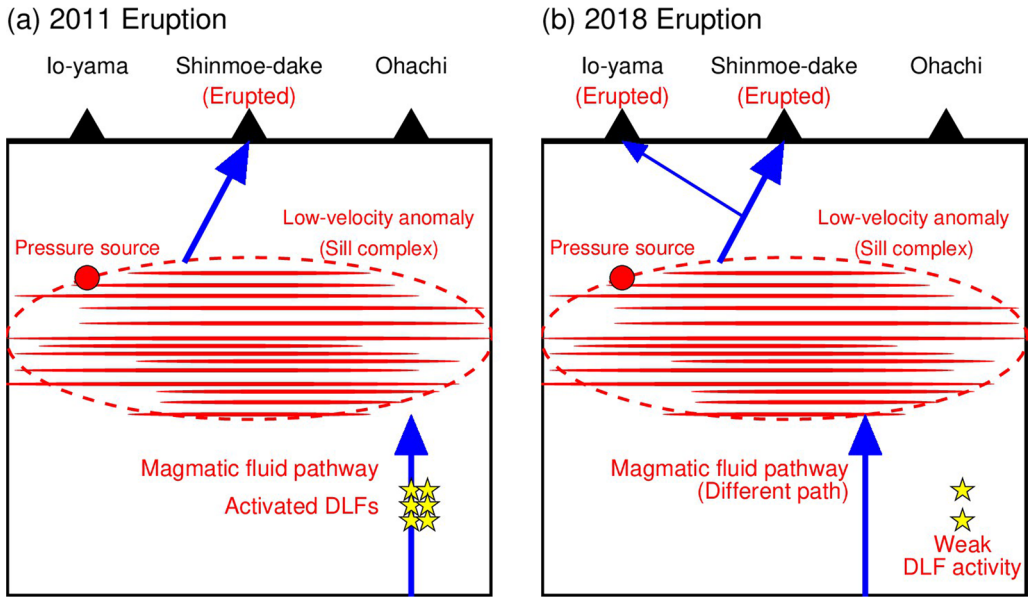

Introduction

Deep low-frequency (DLF) earthquakes, whose waveforms possess dominant frequencies in the 1–8 Hz range, occur at 10–50 km in volcanic regions. Although the relationship between DLF earthquakes and volcanic activity is not well-understood for many volcanoes, recent studies have revealed a potential relationship between DLF earthquakes and surface volcanic activity, such as an eruption. For example, DLF earthquakes increased before and after the eruptions at Klyuchevskoy volcano, Kamchatka, Russia (Shapiro et al. 2017; Frank et al. 2018) and Hakone volcano, Japan (Yukutake et al. 2019). These observations suggest that increased DLF earthquake activity may be the footprint of a deep magmatic fluid supply, which ultimately culminates in surface volcanic activities, such as eruptions and crustal deformation.

The Kirishima volcanic complex is one of the most active volcanic complexes in Japan. Numerous studies have investigated the overall magma supply system of this volcanic complex (e.g., Tajima et al. 2022). Seismic tomography and seismic interferometry studies have imaged low-velocity anomalies beneath the volcanic complex, with one located at 10–15 km depth (e.g.,Yamamoto and Ida 1994; Nagaoka 2020) and another located at 25–35 km depth (Zhao et al. 2018). These low-velocity anomalies are inferred to correspond to magma reservoirs. Furthermore, a magnetotelluric survey has imaged conductors at depths of 10–15 km, which roughly corresponds to the shallow low-velocity anomaly, and conductive pathways from these conductors to the surface at Shinmoe-dake and Io-yama (Aizawa et al. 2014). Petrological studies have suggested that magma mixing occurred before the 2011 eruptions (Suzuki et al. 2013; Tomiya et al. 2013).

In Kirishima volcano, DLF earthquakes occur at the two depths of 10–15 km and 20–25 km (Kurihara et al. 2019). In the previous study, the number of DLF earthquakes at the depths of 25 km increased before and after the 2011 Shinmoe-dake eruptions. Therefore, DLF earthquake activity at 25 km depth is an important clue for the existence of a deep magma supply system beneath the Kirishima volcanic complex. DLF earthquake activity started in December 2009, coincident with the beginning of the surface crustal deformation associated with inflation of the magma reservoir at 10 km depth. There was a high occurrence rate of DLF earthquake activity until September 2011, which was after the main Shinmoe-dake eruptions in January 2011, with swarm activity accompanying some of the eruptions. Furthermore, the waveforms for the 2009–2011 DLF earthquakes are richer in low-frequency component than those for other periods, which suggests that crustal fluids may have influenced the excitation of these DLF earthquakes. Therefore, deep magmatic fluids may have played an important role in the 2011 Shinmoe-dake eruptions.

Kurihara et al. (2019) also analyzed the DLF earthquake activity during the 2018 Shinmoe-dake and Io-yama eruptions and reported that there were minimal

changes in the occurrence rate of DLF earthquake activity associated with the 2018 eruptions. However, the study only used template DLF earthquakes from the 2004–2015 period for DLF earthquake detection based on the matched-filter technique, with no inclusion of the 2017–2018 DLF earthquake activity during the template selection process. The lack of template events from the target analysis period may be the reason for the apparent low rate of DLF earthquake activity associated with the 2018 eruptions. In addition, because DLF earthquakes generally have small waveform amplitudes, they can be identified from waveforms recorded only at stations with high signal-to-noise (SN) ratios. Previous studies demonstrate that the SN-ratio of station N.SUKH is the highest around the Kirishima volcano (Kurihara et al. 2019, 2021). Thus, template matching using waveform at the single station N.SUKH is expected to lead to a more comprehensive detection of DLF earthquakes compared to the previous studies.

Here, we apply a new matched-filter technique that was developed by Kurihara et al. (2021) to the continuous waveform data surrounding the 2018 eruptions, with a sufficient number of template events employed for DLF earthquake detection, to more accurately capture the temporal variations in DLF earthquake activity. Furthermore, we conduct the same analysis on the waveforms associated with the 2011 eruptions. We suggest that deep pathways for magmatic fluid ascension are different for the 2011 and 2018 eruptions based on a comparison of the temporal evolutions of DLF earthquake activity associated with these two eruptions. The occurrence rate of DLF earthquake activity may depend on the distance between the deep magma fluid supply pathway and the source area hosting DLF earthquakes.

Data and methods

We applied a new matched-filter technique that was developed by Kurihara et al. (2021), which uses the product of the mutual information (MI) and correlation coefficient (CC) for earthquake detection (the product is called as "MICC" in below), to the continuous data recorded at a single seismic station (N.SUKH in Fig. 1). We applied a 1–8-Hz bandpass filter, 25-Hz sampling frequency, and 8-s window length to the waveforms prior to the analysis, as outlined in Kurihara et al. (2021). We employed 293 DLF earthquakes from the April 2004–December 2018 period in the JMA catalog as template events.

In the calculation of MICC, we normalize the waveforms within each 8-s time window using its maximum absolute amplitude. We then assigned the normalized velocities of each time step in each time window, $\overline{v}_{\mathrm{tp}}(t)$ and $\overline{v}_{\mathrm{tg}}(t)$, as

$$\overline{v}_{\mathrm{tp}}(t) = \frac{v_{\mathrm{tp}}(t)}{\max_t\left(\left|v_{\mathrm{tp}}(t)\right|\right)} \tag{1}$$

and

$$\overline{v}_{\mathrm{tg}}(t) = \frac{v_{\mathrm{tg}}(t)}{\max_t\left(\left|v_{\mathrm{tg}}(t)\right|\right)}. \tag{2}$$

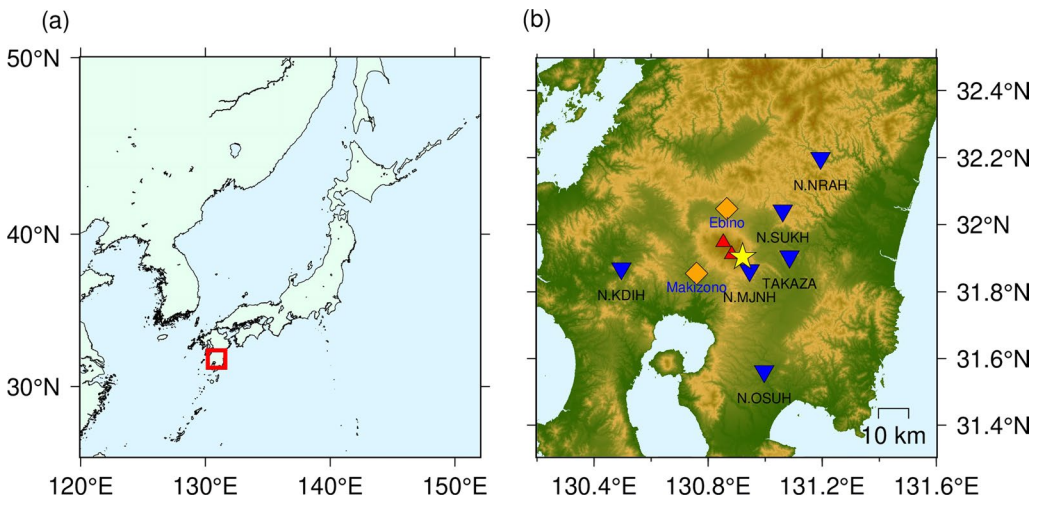

Fig. 1 Map of the Kirishima volcanic complex. **a** Location of Kirishima volcano in Japan. **b** Large view of the Kirishima volcanic complex corresponding to the red rectangle in figure (a). The red triangles indicate the Shinmoe-dake (East) and Io-yama (west). The yellow star marks the primary location of the DLF earthquakes. Blue inverted triangles are seismic stations operated by the National Research Institute for Earth Science and Disaster Resilience (NIED) and Japan Meteorological Agency (JMA), and orange diamonds are the locations of the Ebino and Makizono global navigation satellite system (GNSS) stations, which are operated by the Geospatial Information Authority of Japan (Sagiya 2004)

where the "tg" and "tp" subscripts refer to the velocities of the target and template waveforms, respectively, and the | | notation indicates the absolution value function. We then divide the points in the normalized velocity seismograms into discrete 5×5 cells in the x,y domain. Two integers, n_{tp} and n_{tg}, which indicate the coordinate value of cells between 1 and 5, are given by

$$n_{\mathrm{tp}}(t) = \left\lfloor \left(\overline{v}_{\mathrm{tp}}(t) + 1.4\right) * 2.5 \right\rfloor \quad (\text{when } \overline{v}_{\mathrm{tp}}(t) < 1) \tag{3}$$

$$n_{\mathrm{tg}}(t) = \left\lfloor \left(\overline{v}_{\mathrm{tg}}(t) + 1.4\right) * 2.5 \right\rfloor \quad (\text{when } \overline{v}_{\mathrm{tg}}(t) < 1) \tag{4}$$

$$n_{\mathrm{tp}}(t) = 5 \quad (\text{when } \overline{v}_{\mathrm{tp}}(t) = 1) \tag{5}$$

$$n_{tg}(t) = 5 \quad \left(\text{When } \overline{v}_{tg}(t) = 1\right), \tag{6}$$

where the ⌊ ⌋ notation indicates the floor function.

We then used these integers for the calculation of MI:

$$\mathrm{MI}(t) = \sum_{n_{\mathrm{tp}}=1}^{5} \sum_{n_{\mathrm{tg}}=1}^{5} p\left(n_{\mathrm{tp}}, n_{\mathrm{tg}}\right) \log \frac{p\left(n_{\mathrm{tp}}, n_{\mathrm{tg}}\right)}{p\left(n_{\mathrm{tp}}\right) p\left(n_{\mathrm{tg}}\right)} \tag{7}$$

where p indicates the probability density function. Here, we defined the function $p(n_{tg}, n_{\mathrm{tg}})$ by dividing the number of points corresponding to each time steps in each 5×5 cell by the total number of the time steps (200). We defined the information entropies, h_{tp} and h_{tg}, as

$$h_{\mathrm{tp}} = \sum -p\left(n_{\mathrm{tp}}\right) \log p\left(n_{\mathrm{tp}}\right) \tag{8}$$

and

$$h_{\mathrm{tg}} = \sum -p\left(n_{\mathrm{tg}}\right) \log p\left(n_{\mathrm{tg}}\right), \tag{9}$$

respectively. We then normalized MI as

$$\overline{\mathrm{MI}} = \frac{2.0 * \mathrm{MI}}{h_{\mathrm{tp}} + h_{\mathrm{tg}}}. \tag{10}$$

We hereafter simply describe $\overline{\mathrm{MI}}$ as MI. This value shows the similarity of normalized velocity of the target and template events. MI reflects similarities of waveform portions with amplitudes close to zero, where CC is less sensitive generally.

We calculated the CC of component j at seismic station i for time t as

$$\mathrm{CC}_{ij}(t) = \frac{\sum_{\tau} \left(v_{ij}^{\mathrm{tp}}(t_{\mathrm{tp}} + \Delta t_i + \tau) v_{ij}^{\mathrm{tg}}(t + \Delta t_i + \tau) \right)}{\sqrt{\sum_{\tau} \left(v_{ij}^{\mathrm{tp}}(t_{\mathrm{tp}} + \Delta t_i + \tau) \right)^2} \sqrt{\sum_{\tau} \left(v_{ij}^{\mathrm{tg}}(t + \Delta t_i + \tau) \right)^2}}, \tag{11}$$

where Δt_{i} is the time delay from the origin time of the template earthquakes to S-wave arrival time at station i and τ means the time steps in the time window. Here, we define the MICC index, which is the product of MI and CC, as

$$\mathrm{MICC}(t) = \mathrm{MI}(t)\mathrm{CC}(t). \tag{12}$$

MICC combines two characteristics of MI, which can evaluate the similarity of waveforms in the small amplitude portion, and CC, which is generally sensitive to the large amplitude portion of the waveforms (cf. Kurihara et al. 2021).

We then employed the MICC index for our DLF earthquake detection. We set the MICC threshold at 0.35 for our DLF earthquake detection, following Kurihara et al. (2021). We avoided multiple detections by only including the detection with the highest MICC in a given 10-s time window. Furthermore, we removed any misdetections from surface waves of teleseismic events based on the average amplitudes of the 0–10-s and 10–20-s time windows after the S-wave arrival time, with the potential mis-detections automatically removed when the average amplitude in the 10–20-s window was larger than that in the 0–10-s window. The magnitude of each detected event was calculated based on the average root-mean-square velocities between the detected event and the template event among all of the channels:

$$\mathrm{Mj}_{\mathrm{detect}} = \mathrm{Mj}_{\mathrm{temp}} + \frac{1}{0.85} \log \left(\frac{V_{\mathrm{detect}}}{V_{\mathrm{temp}}} \right), \tag{13}$$

where $\mathrm{Mj}_{\mathrm{detect}}$ and $\mathrm{Mj}_{\mathrm{temp}}$ are the JMA magnitudes of the detected and template events, respectively, and V_{detect} and V_{temp} are the root-mean-square velocities of the detected and template events in the 8-s time window, respectively.

We recognized that misdetections from surface waves of teleseismic events and near-surface harmonic tremors (e.g., Natsume et al. 2019) were included in the detections after applying the MICC-based matched-filter method to single station data (Additional file 1: Figs. S1 and S2), even though we automatically removed some misdetections. In particular, many near-surface harmonic tremors were detected on the days of the eruptions; i.e., 6 and 7 March 2018. We visually inspected waveforms for all of the detected events from the 2010–2011 and 2017–2018

periods that were recorded by multiple stations around the Kirishima volcanic complex (Hi-net stations operated by NIED and a seismic station operated by JMA; Fig. 1). We then carefully selected the most robust events by focusing on the event duration, the amplitude ratio between horizontal and vertical components, the arrival time at each station, and the waveform amplitude. Finally, we constructed more precise catalogs of the 2010–2011 and 2017–2018 DLF earthquakes than the automatically constructed catalog.

Results and discussion

A total of 75 DLF earthquakes were identified during the 2017–2018 period (Fig. 2), and 1302 events were identified during the 2010–2011 period (Fig. 3). The temporal changes in DLF earthquake activity are qualitatively similar to those of the original catalog, which was automatically constructed without any visual inspection (Additional file 1: Figs. S1 and S2). Although the number of 2017–2018 DLF earthquakes is small, we can see two major characteristics associated with the DLF earthquake activity (Fig. 2). The first characteristic is two temporal DLF earthquake clusters in March and July 2017. Tajima et al. (2020) reported that two mud pots appeared in March 2017 and two jet fumaroles appeared in April 2017. Ohba et al. (2021) reported that the chemical composition of the volcanic gasses changed in May 2017, indicating increases in SO_2 and H_2 concentrations. Based on these observations, there may be potential links between DLF earthquake activation at 25 km depth and these surface volcanic activities. Furthermore, the DLF earthquake cluster in July 2017 coincided with the initiation of crustal deformation, indicating inflation of the magma reservoir. Similar DLF earthquake activity that was associated with crustal deformation was also observed in December 2009, prior to the 2011 eruptions (Kurihara et al. 2019).

The second characteristic is the slight increase in the occurrence rate of DLF earthquake activity after the eruptions in March 2018. Although only a few DLF earthquakes occurred in 2017, with the exception of the two above-mentioned clusters, DLF earthquake activity continued at an approximately constant rate (three DLF earthquakes per month) after the 2018 eruptions. The present result suggests that the increase in DLF

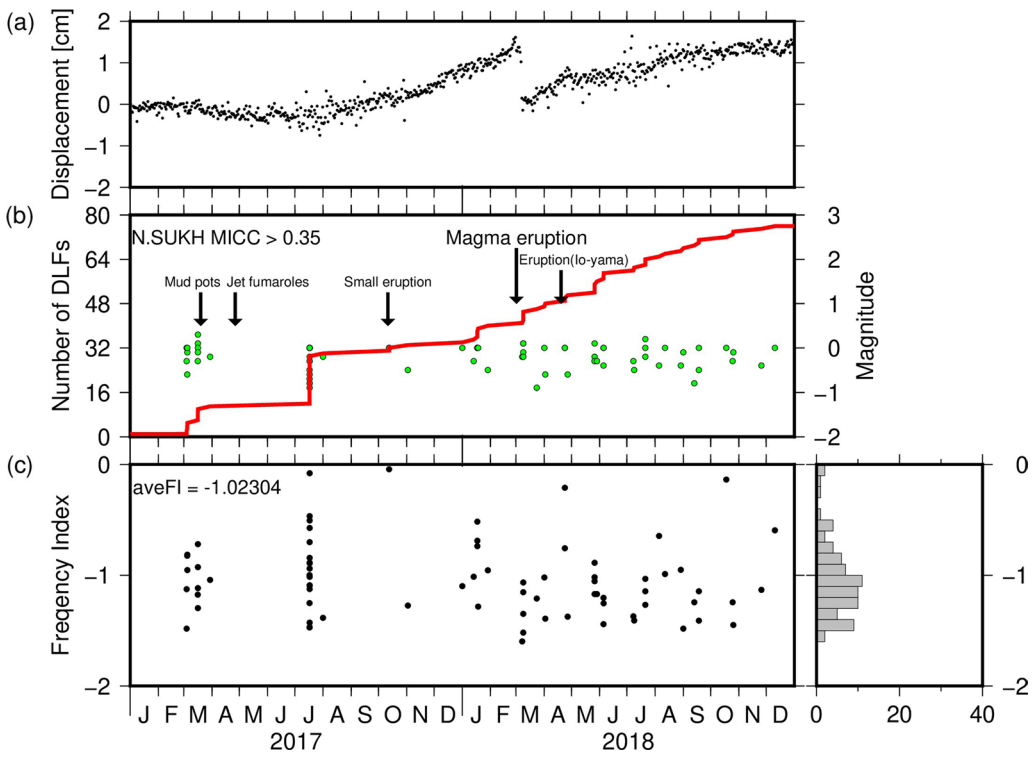

Fig. 2 Geodetic and DLF earthquake observations in the Kirishima volcanic complex during the 2017–2018 period. **a** Horizontal displacement at Ebino GNSS station relative to Makizono (see Fig. 1). We use the F3 solutions provided by the Geospatial Information Authority of Japan. **b** Cumulative number of DLF earthquakes (red line) and DLF earthquake magnitudes (green circles). The DLF earthquakes were selected after visual inspection. Arrows mark the timings of appearances of mud pots and jet fumaroles (Tajima et al. 2020), as well as the eruptions. **c** Frequency index (FI) of the DLF earthquakes. The right panel shows the FI frequency distribution

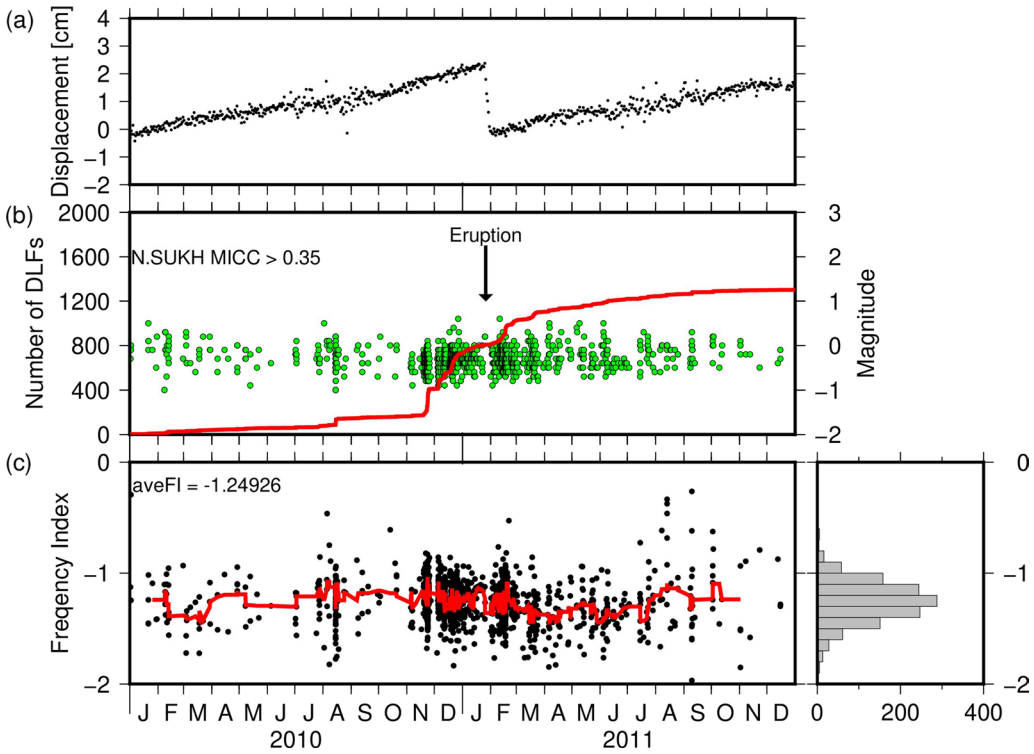

Fig. 3 Geodetic and DLF earthquake observations in the Kirishima volcanic complex during the 2010–2011 period. **a** Horizontal displacement at Ebino GNSS station relative to Makizono (see Fig. 1). **b** Cumulative number of DLF earthquakes (red line) and DLF earthquake magnitudes (green circles). **c** Frequency index (FI) of the DLF earthquakes. The median FI value (red line) is based on a moving window of 15 events. The right panel shows the FI frequency distribution

earthquakes associated with surface volcanic activity may be affected by supply of deep magmatic fluids. The ascent of deep magmatic fluids from 25 km depth may have induced the DLF earthquakes and subsequently culminated in the surface eruptions.

One of the important results of the previous study (Kurihara et al. 2019) was that the 2010–2011 DLF earthquakes have lower dominant frequencies than those of DLF earthquakes in other periods, including 2017–2018 eruption periods. The dominant frequencies of the 2010–2011 DLF earthquakes were lower than those in the other periods. However, the dominant frequencies of the 2017–2018 DLF earthquakes do not have such a low-frequency characteristic. Although some of the DLF earthquakes have lower frequency components, other DLF earthquakes have higher frequency components. We quantified the waveform characteristics using the frequency index (FI). We computed the power spectrum using the 8-s time window after the S-wave arrival time via Fourier transformation and calculated FI based on the ratio of the 1–2-Hz and 4–8-Hz spectra as

$$\mathrm{FI} = \log_{10}\left(\frac{\mathrm{Averagedspectrum4-8Hz}}{\mathrm{Averagedspectrum1-2Hz}}\right). \tag{14}$$

Equation (14) indicates that DLF earthquakes with low dominant frequencies have small FI values. Almost all of the DLF earthquakes associated with the 2011 eruptions possess FI below − 1.0 (Fig. 3c), which highlights the radiation of predominantly lower frequency energy from the 2010–2011 DLF earthquakes. However, some of the DLF earthquakes associated with the 2018 eruptions possess FI above − 1.0 (Fig. 2c), which highlights that the energy radiating from the 2017–2018 DLF earthquakes eruptions possessed a relatively large high-frequency component. For example, the cluster in July 2017 included DLF earthquakes possessing a broad range of FI values, thereby indicating that these events possessed a broad range of dominant frequencies. These observations highlight different DLF earthquake characteristics between the 2011 and 2018 eruptions (Fig. 4).

The magma supply system of the Kirishima volcanic complex proposed by Tajima et al. (2022) and Nishida et al. (2020) includes a low-velocity anomaly at 10–15 km

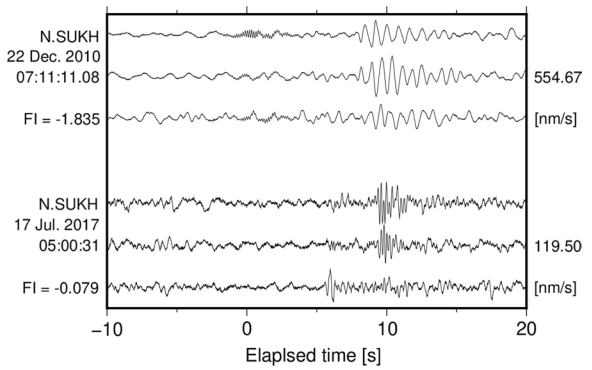

Fig. 4 Waveform examples of DLF earthquakes. Top three component waveforms show an DLF earthquakes in 2010 with the low FI value (FI = − 1.835). Bottom three component waveforms show an DLF earthquakes in 2017 with the high FI value (FI = − 0.079). These waveforms were normalized by the maximum value written on the right side of the box

depth (Yamamoto and Ida 1994; Nagaoka 2020) and a crustal deformation pressure source at 10 km depth (Nakao et al. 2013). The ejected silicic magma in the 2011 eruptions had been stored at 5 km depth (Suzuki et al. 2013). A key difference between the 2011 and 2018 eruptions is that Io-yama only erupted in 2018 (Fig. 4). Aizawa et al. (2014) suggested that magma may be supplied along pathways from a conductor at 10 km depth to Io-yama and Shinmoe-dake, based on broadband magnetotelluric measurements. Ohba et al. (2021) concluded that magma sealing beneath Io-yama and magma transport to Shinmoe-dake occurred simultaneously in 2011. These results suggest that the 2018 Io-yama eruptions were triggered by volcanic phenomena at 5–10 km depth. The present study reveals that a deep magma supply was present during both the 2011 and 2018 eruptions. In this way, we consider the model of magma supply system.

It is very important result that the activity level and waveform characteristics of the DLF earthquakes were notably different during the 2011 and 2018 eruptions. If the magma supply rate of the 2018 eruption had been lower than that of the 2011 eruption, the amount of surface deformation in 2018 would be much smaller than that in 2011. However, the observed crustal deformation in 2018 is similar in scale to that in 2011 (Figs. 2a and 3a), while the activities of DLF earthquakes are markedly different (Figs. 2b and 3b). Therefore, we propose a model that the magmatic fluids for these two eruptions were potentially supplied along different pathways to explain the different DLF behaviors, as shown in Fig. 5. The magmatic fluids that supplied the 2011 eruptions may have ascended through a pathway near the source regions of the DLF earthquakes, which induced fluid oscillations, resulting in the generation of many DLF earthquakes. Conversely, the magmatic fluids that supplied the 2018 eruptions may have ascended along a pathway away from the source region of the DLF earthquakes, resulting in the

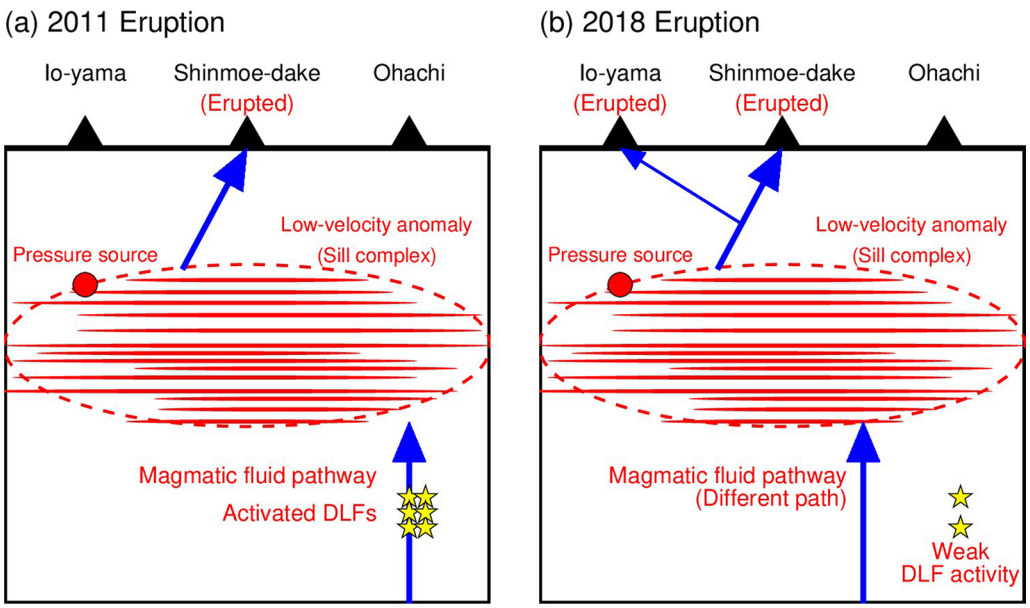

Fig. 5 Model of deep magma supply path and ascension of magmatic fluids during the **a** 2011 and **b** 2018 eruptions (referred as Nishida et al. (2020)). Yellow stars mark the DLF earthquake hypocenters. Blue arrows indicate the magmatic fluid pathways. The large red ellipse denotes the low-velocity anomaly, which has been interpreted to represent magmatic sills (Nagaoka 2020). The solid red circle marks the location of measured crustal deformation in 2011 (Nakao et al. 2013), and it may be similar to the eruption of 2018 (Geospatial Information Authority of Japan 2018)

weak activation of DLF earthquakes. This weak DLF earthquake activity was likely due to either a limited stress transfer from the ascending magmatic fluids or limited infiltration of the fluids into the source region. Although the connection between deep magma supply and the Io-yama eruptions is unknown, the magma supply process for both the 2011 and 2018 eruptions may differ in both the shallower (< 10 km) and deeper (15–30 km) parts of the magmatic fluid pathways. Furthermore, the time lag between the onset of DLF earthquake activity and the shallow volcanic unrest is very short, as seen in the 2011 eruptions (Kurihara et al. 2019). These observations suggest that the pressure perturbation associated with the magma supply may have propagated rapidly from deep to shallow depths through volcanic conduits. However, it is difficult to specify the detailed process of this pressure perturbation due to limited constraints on the deep volcanic structure. A combination of geophysical, geochemical, and petrological observations is necessary to fully characterize the magma supply system beneath Kirishima volcanic complex.

Conclusions

We investigated the DLF earthquake activity surrounding the 2018 Shinmoe-dake and Io-yama eruptions of the Kirishima volcanic complex by applying a matched-filter method to the continuous seismic data recorded at a single station and manually inspecting all of the earthquake detections. Although the total DLF earthquake activity associated with the 2018 eruptions was much weaker than that for the 2011 eruptions, the temporal evolution of DLF earthquake activity was consistent with the surface-induced volcanic unrest and crustal deformation observations. This result suggests that a deep magma supply influenced both the 2011 and 2018 eruptions. The magma from this deep supply may have ascended along different pathways during the 2011 and 2018 eruptions owing to the differences in activity levels and waveform characteristics of the DLF earthquakes during the two eruptions.

Abbreviations

DLF: Deep low-frequency; GNSS: Global navigation satellite system; CC: Correlation coefficients; MI: Mutual information; MICC: Product of mutual information and correlation coefficients; Hi-net: High-sensitivity seismograph network; NIED: National Research Institute for Earth Science and Disaster Resilience; JMA: Japan meteorological agency; JST: Japan Science and Technology Agency; CREST: Core Research for Evolutional Science and Technology; JSPS: Japan Society for the Promotion of Science.

Supplementary Information

The online version contains supplementary material available at https://doi.org/10.1186/s40623-022-01723-1.

Additional file 1: Figure S1. (a) Amount of the horizontal displacement of Ebino relative to Makizono (see Fig. 1) calculated from GNSS data in 2017–18. We use F3 solutions provided by Geospatial Information Authority of Japan. (b) Cumulative number of DLF earthquakes (red line) and magnitude of DLF earthquakes (green circle) for all events automatically detected. (c) Frequency index (FI) of DLF earthquakes. **Figure S2.** a) The amount of the horizontal displacement of Ebino relative to Makizono (see Fig. 1) calculated from GNSS data in 2010–2011. We use F3 solutions provided by Geospatial Information Authority of Japan. (b) Cumulative number of DLF earthquakes (red line) and magnitude of DLF earthquakes (green circle). (c) Frequency index (FI) of DLF earthquakes and median value of FI in a moving window with the 15 events (7 events before the target event and 7 events after the target event) window.

Acknowledgements

We used Generic Mapping Tools to produce the figures (Wessel and Smith 1998). We collated the Hi-net seismic observation data (http://www.hinet.bosai.go.jp) from NIED (National Research Institute for Earth Science and Disaster Resilience 2019) and used JMA's unified earthquake catalog (http://www.jma.go.jp) for the presented analysis. We used the computer systems at the Earthquake and Volcano Information Center of the Earthquake Research Institute, the University of Tokyo, for data processing and analysis. This work was supported by the JST CREST (Grant Number JPMJCR1763), JSPS KAKENHI grant number 22K14113, and the Ministry of Education, Culture, Sports, Science and Technology (MEXT) of Japan, under its The Second Earthquake and Volcano Hazards Observation and Research Program (Earthquake and Volcano Hazard Reduction Research). We thank Dr. Naofumi Aso and the anonymous reviewer for helpful comments.

Author contributions

RK designed the study and analyzed the data. AK advised and discussed the contents of the study. Both authors wrote the manuscript. Both authors read and approved the final manuscript.

Funding

This work was mainly supported by Japan Science and Technology Agency (JST) CREST Grant Number JPMJCR1763, and partially supported by JSPS (Japan Society for the Promotion of Science) KAKENHI Grant Number 22K14113.

Availability of data and materials

We used the Hi-net seismic observation data from NIED (National Research Institute for Earth Science and Disaster Resilience 2019) and the JMA unified earthquake catalog, which are available from the NIED Hi-net website (http://www.hinet.bosai.go.jp).

Declarations

Ethics approval and consent to participate

Not applicable.

Consent for publication

Not applicable.

Competing interests

The authors declare that they have no competing interests.

Author details

[1]Earthquake Research Institute, The University of Tokyo, 1-1-1 Yayoi, Bunkyo, Tokyo 113-0032, Japan. [2]Present Address: Hot Springs Research Institute of Kanagawa Prefecture, 586 Iryuda, Odawara, Kanagawa 250-0031, Japan.

Received: 7 August 2022 Accepted: 16 October 2022
Published online: 30 November 2022

References

Aizawa K, Koyama T, Hase H et al (2014) Three-dimensional resistivity structure and magma plumbing system of the Kirishima Volcanoes as inferred from

broadband magnetotelluric data. J Geophys Res Solid Earth 119:198–215. https://doi.org/10.1002/2013JB010682
Frank WB, Shapiro NM, Gusev AA (2018) Progressive reactivation of the volcanic plumbing system beneath Tolbachik volcano (Kamchatka, Russia) revealed by long-period seismicity. Earth Planet Sci Lett 493:47–56. https://doi.org/10.1016/j.epsl.2018.04.018
Geospatial Information Authority of Japan (2018) Crustal Deformations around Kirishima Volcano. Rep Coord Comm Predict Volcan Erupt 130:324–347
Kurihara R, Obara K, Takeo A, Tanaka Y (2019) Deep low-frequency earthquakes associated with the eruptions of Shinmoe-dake in KirishimaVolcanoes. J Geophys Res Solid Earth 124:13079–13095. https://doi.org/10.1029/2019JB018032
Kurihara R, Kato A, Kurata S, Nagao H (2021) Detection of low-frequency earthquakes by the matched filter technique using the product of mutual information and correlation coefficient. Earth Planets Space. https://doi.org/10.1186/s40623-021-01534-w
Nagaoka Y (2020) Study on seismic velocity structure beneath active volcanoes by seismic interferometry. PhD thesis, Univ Tokyo
Nakao S, Morita Y, Yakiwara H et al (2013) Volume change of the magma reservoir relating to the 2011 Kirishima Shinmoe-dake eruption—charging, discharging and recharging process inferred from GPS measurements. Earth Planets Space 65:505–515. https://doi.org/10.5047/eps.2013.05.017
National Research Institute for Earth Science and Disaster Resilience (2019) NIED Hi-net. Natl Res Inst Earth Sci Disaster Resil. https://doi.org/10.17598/nied.0003
Nishida K, Mizutani Y, Ichihara M, Aoki Y (2020) Time-lapse monitoring of seismic velocity associated with 2011 Shinmoe-dake eruption using seismic interferometry: an extended Kalman Filter approach. J Geophys Res Solid Earth 125:1–23. https://doi.org/10.1029/2020JB020180
Ohba T, Yaguchi M, Tsunogai U et al (2021) Behavior of magmatic components in fumarolic gases related to the 2018 phreatic eruption at Ebinokogen Ioyama volcano, Kirishima Volcanic Group, Kyushu, Japan. Earth Planets Space. https://doi.org/10.1186/s40623-021-01405-4
Sagiya T (2004) A decade of GEONET: 1994–2003—The continuous GPS observation in Japan and its impact on earthquake studies. Earth Planets Space 56:xxix–xli. https://doi.org/10.1186/BF03353077
Shapiro NM, Droznin DV, Droznina SY et al (2017) Deep and shallow long-period volcanic seismicity linked by fluid-pressure transfer. Nat Geosci 10:442–445. https://doi.org/10.1038/ngeo2952
Suzuki Y, Yasuda A, Hokanishi N et al (2013) Syneruptive deep magma transfer and shallow magma remobilization during the 2011 eruption of Shinmoe-dake, Japan—Constraints from melt inclusions and phase equilibria experiments. J Volcanol Geotherm Res 257:184–204. https://doi.org/10.1016/j.jvolgeores.2013.03.017
Tajima Y, Nakada S, Maeno F et al (2020) Shallow magmatic hydrothermal eruption in April 2018 on Ebinokogen Ioyama Volcano in Kirishima Volcano Group, Kyushu, Japan. Geosciences 10:183. https://doi.org/10.3390/geosciences10050183
Tajima Y, Oikawa J, Kobayashi T, Yasuda A (2022) Middle to long-term magma pdoduction activities and the plumbing system of Shinmoedake, Kirishima volcano: toward a unified understanding based on products analyses and geophysical observations. Bull Volcanol Soc Japan 67:45–68. https://doi.org/10.18940/kazan.67.1.45
Tomiya A, Miyagi I, Saito G, Geshi N (2013) Short time scales of magma-mixing processes prior to the 2011 eruption of Shinmoedake volcano, Kirishima volcanic group. Japan Bull Volcanol 75:750. https://doi.org/10.1007/s00445-013-0750-1
Wessel P, Smith WHF (1998) New, improved version of generic mapping tools released. Eos, Trans Am Geophys Union 79:579–579. https://doi.org/10.1029/98EO00426
Yamamoto K, Ida Y (1994) Three-dimensional P-wave velocity structure of Kirishima volcanoes using regional seismic events. Bull Earthq Res Inst Univ Tokyo 69:267–289
Yukutake Y, Abe Y, Doke R (2019) Deep low-frequency earthquakes beneath the Hakone Volcano, Central Japan, and their relation to volcanic activity. Geophys Res Lett. https://doi.org/10.1029/2019GL084357
Zhao D, Yamashita K, Toyokuni G (2018) Tomography of the 2016 Kumamoto earthquake area and the Beppu-Shimabara graben. Sci Rep 8:1–11. https://doi.org/10.1038/s41598-018-33805-0

Publisher's Note